Topologically Multicharged and Multihumped Rotating Solitons in Wide-Aperture Lasers With a Saturable Absorber

Sergey V. Fedorov, Nikolay N. Rosanov, Anatoly N. Shatsev, Nikolay A. Veretenov, and Andrei G. Vladimirov

Invited Paper

***Abstract*—We present results of a semianalytical and numerical study of transverse two-dimensional stationary and oscillating solitons in a wide-aperture laser with a saturable absorber and fast nonlinearity of both gain and absorption. We determine the stability conditions and bifurcations of axially symmetric solitons with screw wavefront dislocations of different order. We demonstrate the existence of asymmetric rotating laser solitons with different numbers of intensity maxima.**

***Index Terms*—Lasers, nonlinear optics, optical bistability, optical solitons.**

I. Introduction

DISSIPATIVE optical solitons are self-organized light beams created by hard (threshold-type) excitation in nonlinear optical media or schemes with a balance between optical energy losses and gain. The requirement of energy balance results in a discrete spectrum of the main parameters of dissipative solitons, as distinct from the continuous spectrum of more familiar conservative optical solitons, e.g., in fibers with a nonlinear refractive index [1]–[3]. This important difference is interesting not only from a fundamental standpoint. The robustness of the dissipative optical solitons and the suppression of noise due to the threshold character of their excitation open up perspectives of their possible applications in optical information processing.

There are a number of optical schemes in which dissipative solitons exist. The dissipative optical solitons were first found theoretically in wide-aperture nonlinear driven interferometers [4], [5]. Experimentally, they were first demonstrated in a liquid-crystal valve scheme with spatial filtering in the feedback [6], [7]. Another example of such "driven" schemes in which dissipative solitons exist is a single-mirror feedback system containing a cell with Na vapor [8]. There are also schemes without the external signal, such as wide-aperture lasers with a saturable absorber. *Laser solitons* in such schemes were predicted in [9], [10] (see also [11]). Subsequent theoretical and experimental studies of dissipative optical solitons are summarized in a number of recent reviews [12]–[20].

Both "driven" (passive) and "laser" schemes are especially promising for applications when based on semiconductor microcavities with multiple quantum wells or dots [21], [22]. The main difference between dissipative solitons in passive and active schemes is the following. Stationary solitons in driven schemes have the frequency of the external signal and are phase-matched with it, whereas the frequency of a stationary laser soliton is the unknown eigenvalue of the problem, and its phase is arbitrary. Note also that feedback is not a prerequisite for the existence of the laser soliton. Localized structures described by equations similar to laser equations can be created in a continuous medium, planar waveguide, or fiber with nonlinear gain and absorption. Therefore, the term *cavity soliton* is not appropriate here. As a consequence, laser solitons are extremely diverse. (For a review of features of one-, two-, and three-dimensional (1-, 2-, and 3-D) laser solitons, see [20].) Also highly diversified are the scenarios of laser soliton stability loss and generation of new structures.

Our aim is to present a systematic semianalytical and numerical study of the stability and bifurcations of transversely 2-D solitons characterized by different topological charges (localized vortices of different order) in a wide-aperture laser with an intracavitary nonlinear absorber. We also demonstrate the existence of rotating asymmetric "multihumped" solitons with different numbers of intensity maxima.

In Section II, we describe the laser model, present the governing equation, and discuss its symmetries. In Section III, we study stationary localized structures with axially symmetric intensity distribution, including localized vortices of different order. We analyze their stability with respect to small perturbations. In Section IV, we present the results of numerical solutions of the governing equation. We describe the bifurcations of the symmetric laser vortices, the appearance of new types of laser solitons, asymmetric and nonstationary ones, and hysteresis phenomena in which all these types of solitons

Manuscript received June 4, 2002; revised October 21, 2002. This work was supported by the Russian Foundation for Basic Research under Grant 02-02-81045.

S. V. Fedorov, N. N. Rosanov, and A. N. Shatsev are with the Theoretical Department, Research Institute for Laser Physics, St. Petersburg 199034, Russia (e-mail: sfedorov@sf3997.spb.edu; rosanov@ilphs.pb.su; shatsev@ilph.spb.su).

N. A. Veretenov and A. G. Vladimirov are with the Physics Faculty, St. Petersburg State University, St. Petersburg 198904, Russia (e-mail: werna@mailru.com; andreu@sp1254.spb.edu).

Digital Object Identifier 10.1109/JQE.2002.807212

are involved. In Section V, we briefly discuss some possible generalizations of the model and applications of laser solitons.

II. Laser Model and Equations

We consider a wide-aperture—with a large Fresnel number—laser with an intracavitary saturable absorber. The relaxation times of both gain and absorption are assumed to be small as compared with the field lifetime in the empty cavity t_c (the class-A laser). In the mean-field approximation [23] valid for the case of small variations of the electric-field envelope per one-cavity round trip, the governing equation has the form [20], [24]

$$\frac{\partial E}{\partial t} = (i+d)\Delta_\perp E + Ef\left(|E|^2\right) \tag{1}$$

where E is the dimensionless complex electric-field envelope averaged over the longitudinal coordinate. The dimensionless time t is normalized by t_c. $\Delta_\perp = \nabla_\perp^2 = \partial^2/\partial x^2 + \partial^2/\partial y^2$ is the transverse Laplacian with the dimensionless transverse Cartesian coordinates x and y, normalized by the width of the effective Fresnel zone

$$L_F = \sqrt{\frac{L_c}{2k(1-R)}}. \tag{2}$$

where L_c is the cavity length, k is the light wavenumber, and R is the product of the cavity mirror amplitude coefficients of reflection. The nonlinear function $f(I)$ of the field intensity $I = |E|^2$ describes the fast saturation of gain and absorption. Neglecting frequency detunings, $f(I)$ becomes real and takes the form

$$f\left(|E|^2\right) = -1 + \frac{g_0}{1+|E|^2} - \frac{a_0}{1+b|E|^2} \tag{3}$$

where g_0 and a_0 are small-signal gain and absorption, respectively, and b is the ratio of the saturation intensities for gain and absorption. The nonresonant absorption is rescaled to unity by the time normalization. The "diffusion coefficient" $d \geq 0$ describes a weak spatial dispersion of the optical media and is assumed to be small ($d \ll 1$). Generally, the diffusion coefficient is intensity dependent, but this dependence is absent in the case of zero-frequency detunings [24].

Equation (1) is invariant under a constant phase shift Φ_0 of the electric-field envelope E and also under shifts X_0, Y_0 of the transverse coordinates (translation symmetry)

$$E \to E\exp(i\Phi_0), \quad E(x,y,t) \to E(x+X_0, y+Y_0, t). \tag{4}$$

The existence of these symmetries implies that the soliton possesses the so-called neutral modes, which we will describe in Section III. The symmetry of (1) with respect to rotations of the(x,y) plane can also produce neutral modes. However, in the case of a soliton with axially symmetric intensity distribution, the neutral mode generated by the rotational symmetry coincides with that generated by the phase symmetry. In the numerical simulations below, we fix the following values of parameters: $a_0 = 2$, $b = 10$.

III. Axially Symmetric Laser Solitons

A. Stationary Symmetric Localized Structures

Let us consider a stationary localized structure with an axially symmetric intensity distribution. Then, in polar coordinates (r,φ), $x = r\cos\varphi$, $y = r\sin\varphi$, the electric field is

$$E = A(r)\exp(im\varphi - i\alpha t) \tag{5}$$

where α is the radiation frequency shift with respect to the frequency of transversely homogeneous lasing and an integer m is the topological charge, or azimuthal index. The structures with $m \neq 0$ correspond to localized vortices with screw dislocations of the radiation wavefront. In the vortex center, the field is zero (i.e., $A(0) = 0$). Substituting (5) into (1), we get the following ordinary differential equation for the radial function $A(r)$:

$$\frac{d^2A}{dr^2} + \frac{1}{r}\frac{dA}{dr} + \frac{m^2}{r^2}A + \frac{i\alpha + f\left(|A|^2\right)}{i+d}A = 0 \tag{6}$$

with natural boundary conditions $A(r) \sim r^{|m|}$ at $r \to 0$ and $A(r) \to 0$ at $r \to \infty$. Note that the frequency shift α plays the role of the eigenvalue of the nonlinear problem (6) and has a discrete spectrum. We will use the small-signal gain g_0 as a control parameter. The multicharged localized laser vortices were first found in [25]. More recently, the stability of localized vortices for a nonlaser case with strong diffusion was demonstrated in [26]. In this section, we will find the conditions of their stability, taking into account the effect of weak diffusion.

Prior to the discussion of 2-D structures, note that for 1-D localized laser structures, the dependence of α on g_0 has a spiral-like form [20], [27]. Different coils of the spiral represent structures with different width. Stable laser solitons correspond to some parts of the coils with a negative derivative $d\alpha/dg_0 < 0$ adjacent to the points of saddle-node bifurcation where $|d\alpha/dg_0| = \infty$. The narrowest localized structures corresponding to the first coil can be referred to as "ground-state" laser solitons, whereas wider structures associated with other coils, as "excited" solitons [20], [27], [28]. The dependence of α on g_0 calculated numerically for 2-D axially symmetric structures with topological charges $m = 0, \ldots, 3$ is presented in Figs. 1 and 2. Fig. 1 corresponds to the zero-diffusion coefficient $d = 0$ and Fig. 2 corresponds to $d = 0.1$. Note that the dependence of α on g_0 shown in Fig. 1 is quite different from that obtained in [27] for 1-D localized structures. Instead of an infinite number of coils for the fundamental soliton ($m = 0$), only one spiral coil with a negative derivative $d\alpha/dg_0 < 0$ remains. It is off the scale of Fig. 1. For the localized vortices ($m = 1, 2$), the size of the second coil decreases with the increase of the diffusion coefficient (see Fig. 2). The second coil disappears for $m = 3$ and $d = 0.1$. The first coils corresponding to $m = 1, 2$ are off the scale of both Figs. 1 and 2. In the next section, we analyze the effect of diffusion on the stability of the localized structures.

B. Linear Stability Analysis

It is necessary for the stability of a localized structure that the total linear absorption be greater than the small-signal gain

$$f(0) = -1 - a_0 + g_0 < 0. \tag{7}$$

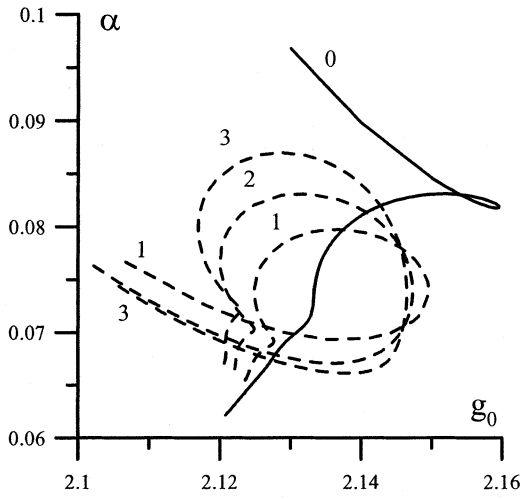

Fig. 1. Spiral-like dependencies of the nonlinear frequency shift α on the small-signal gain g_0 for laser solitons with topological charges $m = 0$ (solid line) and $m = 1,\ 2,\ 3$ (dashed lines). The first coils of the spirals are not shown: they are off the scale. All the vortices are unstable. Diffusion coefficient $d = 0$.

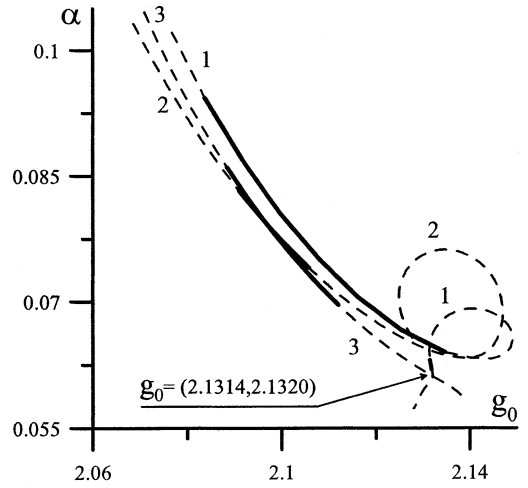

Fig. 2. Dependencies of the nonlinear frequency shift α on the small-signal gain g_0 for laser vortices with $m = 1,\ 2,\ 3$. Diffusion coefficient $d = 0.1$. The vortices are stable within the intervals shown by thick solid lines. The arrow points to the narrow interval of stability of excited solitons with the topological charge $m = 1$.

Otherwise, small peripheral perturbations grow exponentially. The sufficient stability conditions are found by linear stability analysis. We introduce a small perturbation δA by the relation

$$E = [A(r) + \delta A(r, \varphi, t)] \exp(im\varphi - i\alpha t). \tag{8}$$

Then, in polar coordinates, the governing equation (1) (linearized with respect to δA) takes the form

$$\frac{\partial \delta A}{\partial t} = (i + d)\left(\Delta_r^{(m^2)} + \frac{2im}{r^2}\frac{\partial}{\partial \varphi} + \frac{1}{r^2}\frac{\partial^2}{\partial \varphi^2}\right)\delta A + (i\alpha + f_1)\delta A + f_2 \delta A^* \tag{9}$$

where

$$\Delta_r^{(m^2)} = \frac{\partial^2}{\partial r^2} + \frac{1}{r}\frac{\partial}{\partial r} - \frac{m^2}{r^2},\ f_1 = f_0 + f_0' I_0,\ f_2 = f_0' A^2,$$
$$f_0 = f(I_0),\ f_0' = \frac{df}{dI}|_{I=I_0},\ I_0 = |A(r)|^2. \tag{10}$$

We seek the solution of (9) in the form

$$\delta A(r, \varphi, t) = a(r)\exp(i\delta m\varphi + \gamma t) + b^*(r)\exp(-i\delta m\varphi + \gamma^* t), \quad \delta m = 0,\ 1,\ 2, \ldots \tag{11}$$

with the asymptotics $a(r), b(r) \to 0$ at $r \to \infty$. The equation resulting from the substitution of (11) into (9) can be written in matrix form as

$$\mathbf{Lu} = \gamma \mathbf{u}, \quad \mathbf{L} = \begin{pmatrix} a_{11}, & a_{12} \\ a_{21}, & a_{22} \end{pmatrix}, \quad \mathbf{u} = \begin{pmatrix} u_1 \\ u_2 \end{pmatrix}. \tag{12}$$

Here, the components of the matrix operator $\mathbf{L}$ are given by

$$a_{11,22} = \mathrm{Re}(f_1 \pm f_2) - 2im\delta m r^{-2} - d\Delta_r^{(m^2+\delta m^2)}$$
$$a_{12,21} = \mp\alpha \mp \mathrm{Re}(f_1 \mp f_2) \pm 2idm\delta m r^{-2} \mp \Delta_r^{(m^2+\delta m^2)}. \tag{13}$$

The two components of the vector $\mathbf{u}$ are

$$u_1 = a + b, \quad u_2 = i(b - a). \tag{14}$$

The symmetry properties (4) of the governing equation (1) imply the existence of the so-called "neutral modes" which are the eigensolutions of the linearized equation (9) with the zero eigenvalue $\gamma = 0$. Specifically, the symmetry with respect to the phase shift gives rise to the axially symmetric neutral mode $\delta A = iA(r)$ with $\delta m = 0$. The translation symmetry results in the existence of two neutral modes with $\delta m = 1$

$$\delta A_x = \frac{\partial A}{\partial x} = \left(\frac{dA}{dr}\right)\cos\varphi,\ a = b^* = \frac{\frac{dA}{dr}}{2}$$
$$\delta A_y = \frac{\partial A}{\partial y} = \left(\frac{dA}{dr}\right)\sin\varphi,\ a = -b^* = \frac{\frac{dA}{dr}}{2i}. \tag{15}$$

The stability of localized structure is determined by the discrete spectrum of the eigenvalues γ of (12) with a nonzero real part. More precisely, a localized structure is unstable if $\max \mathrm{Re}(\gamma) > 0$, where the maximum is chosen among all the roots of (12). At the bifurcation point, the real part of the critical eigenvalue γ changes its sign. A complex critical eigenvalue with a nonzero imaginary part corresponds to the Andronov–Hopf bifurcation. For $\delta m = 0$, this bifurcation leads to the perturbed structure exhibiting temporal oscillations. Since (11) can be rewritten in the form

$$\delta A(r, \varphi, t) = a(r)\exp[i\delta m(\varphi - \Omega t)] + b^*(r)\exp[-i\delta m(\varphi - \Omega t)] \tag{16}$$

for $\delta m \neq 0$ the rotation of the perturbed structure arises with the rotation angular velocity $\Omega = -\mathrm{Im}\gamma/\delta m$. Note that according to (8) and (11), the field intensity of the rotating structure has δm maxima with the angle φ variation at fixed r and t (a multihumped localized structure).

We have found numerically the eigenvalues γ using discretization of (12) over the radial coordinate r. The results are presented in Figs. 2–7. The axially symmetric localized structures are stable within finite ranges of small-signal gain. The stability range of the fundamental soliton is $2.094 < g_0 < 2.116$ for $d = 0$ (see Fig. 3), and it is only slightly affected by diffusion. The low-gain boundary of the stability range corresponds to the saddle-node bifurcation where stable and unstable localized solutions merge and disappear. At the high-gain boundary of the stability range,

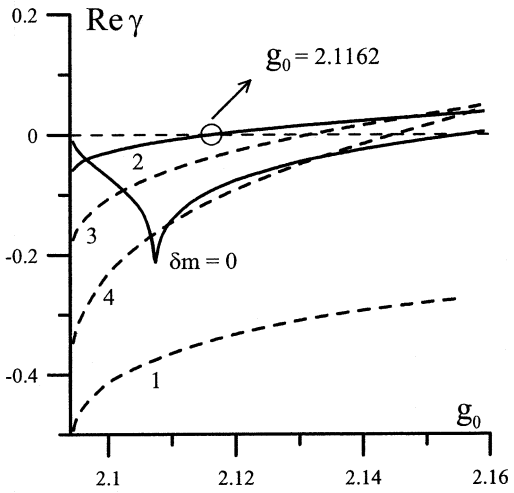

Fig. 3. Dependencies of the small perturbation growth rate Reγ on the small-signal gain g_0 for $m = 0$, $\delta m = 0, 1, 2, 3, 4$, and $d = 0$.

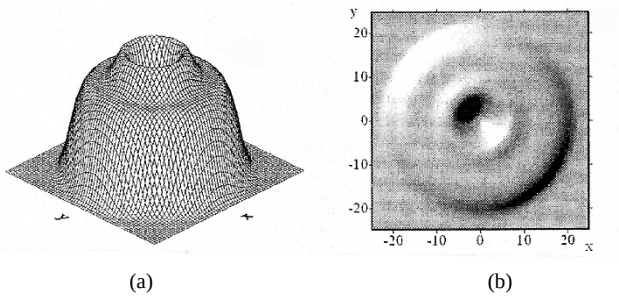

(a) (b)

Fig. 4. (a) Wired surface and (b) surface relief illustrating the transverse distribution of intensity of a stable excited soliton with $m = 1$; $d = 0.06$, $g_0 = 2.129\,776$, and $\alpha = 0.065\,76$.

$g_0 = 2.116$, the fundamental soliton loses its stability due to growth of perturbation harmonics with $\delta m = 2$. In this case, the imaginary part of the critical eigenvalue γ is nonzero; hence, the Andronov–Hopf bifurcation appears. In the framework of the linear stability analysis, it is not possible to determine what regimes are formed after this bifurcation. This question will be considered in the next section.

Unlike the fundamental solitons, all the localized vortices ($m \neq 0$) are unstable for $d = 0$, because there are roots with Re$\gamma > 0$ for the perturbation harmonics with $\delta m = 2$. More precisely, the width of the stability range of a laser localized vortex tends to zero when $d \to 0$. As illustrated in Figs. 2 and 5–7, there are finite ranges of stability of ground-state and excited laser vortices. An example of the transverse intensity distribution corresponding to an excited vortex is given in Fig. 4.

Now let us turn to ground-state vortices that for positive diffusion ($d > 0$) have greater stability ranges than the excited ones. The dependence of the maximum growth rate of perturbations for harmonics with $\delta m = 0, 1, 2, 3$ on small-signal gain is given in Figs. 5–7 for localized vortices with topological charges $m = 1, 2, 3$, respectively. For $d \to 0$, the curve representing the maximum growth rate for $\delta m = 2$ shifts upward. At $d = 0$, it is tangent to the line Re$\gamma = 0$ at a certain value g_0 (see [29, Fig. 5]). There is an additional degeneracy of the eigenvalues of the problem (12) at this value.

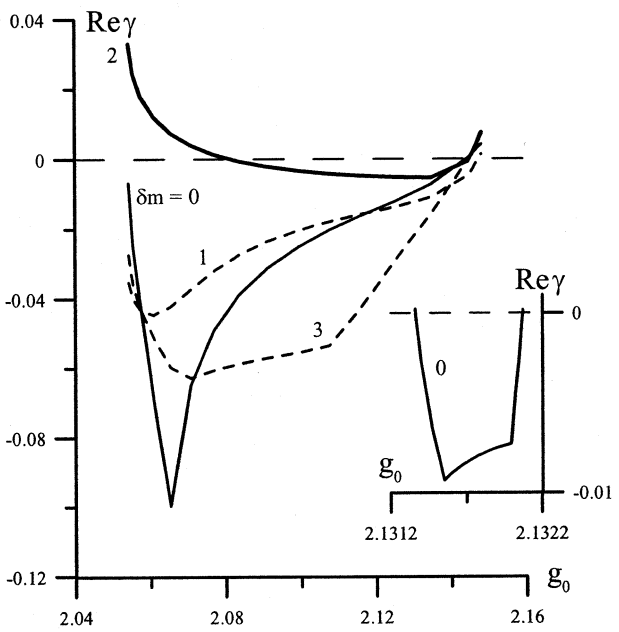

Fig. 5. Dependencies of the small perturbation growth rate Reγ on the small-signal gain g_0 for the perturbation azimuthal harmonics with δm =0–3 for the case of a vortex soliton, $m = 1$. Diffusion coefficient $d = 0.1$. Inset shows the maximum growth rate of perturbations with $\delta m = 0$ for the excited vortex soliton in the narrow interval of its stability (see Fig. 2).

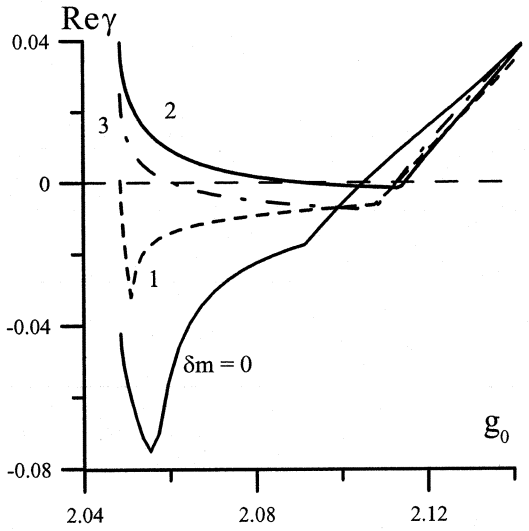

Fig. 6. Dependencies of the small perturbation growth rate Reγ on the small-signal gain g_0 for the perturbation azimuthal harmonics with δm =0–3 for a laser vortex soliton of the second order, $m = 2$, $d = 0.1$.

For the parameters used in our simulations, all the vortices lose their stability with the increase of gain due to the growth of perturbations with $\delta m = 0$, whereas the fundamental soliton is destabilized by the perturbation harmonics with $\delta m = 2$ (see Fig. 3). Since the imaginary part of the critical eigenvalue is nonzero, this instability corresponds to the Andronov–Hopf bifurcation. With the decrease of gain, the vortex solitons with $m = 1, 2$ are destabilized by the perturbations with $\delta m = 2$ (see Figs. 5 and 6). The soliton with $m = 3$ is destabilized by

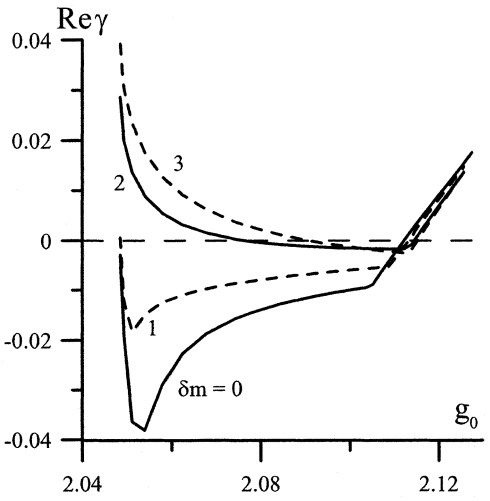

Fig. 7. Dependencies of the perturbation growth rate Reγ on the small signal gain g_0 for a laser vortex of the third order, $m = 3$, $d = 0.1$.

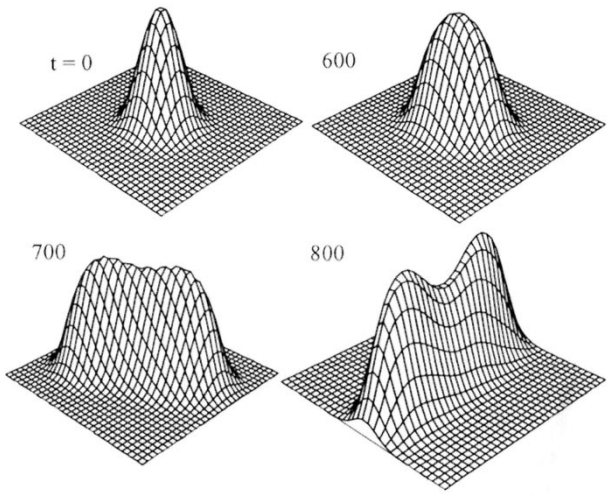

Fig. 8. Transverse intensity distributions illustrating transformation of the axially symmetric soliton ($t = 0$) into an asymmetric rotating soliton with fast increase of the small-signal gain from $g_0 = 2.116$ to 2.14, $d = 0$.

the perturbation harmonics with $\delta m = 3$ (see Fig. 7). This instability results in an intensity distribution of the perturbed soliton with three maxima.

IV. Numerical Simulations

The semianalytical procedure described in the previous sections is incapable of describing localized solutions with axially asymmetric intensity distributions. In order to study these solutions, we need to perform direct numerical simulations of the governing equation (1). In this section, we present the results of such simulations based on the splitting method and the algorithm of the fast Fourier transform [20].

Note that destabilization of a fundamental soliton, $m = 0$, above the high-gain boundary of its stability range is associated with the asymmetric perturbation harmonics with $\delta m = 2$ (see Fig. 3). Numerical calculations confirm the subcritical character of the corresponding Andronov–Hopf bifurcation. With the increase of gain, an initially axially symmetric soliton (Fig. 8, $t = 0$) transforms into a soliton rotating with a constant angular

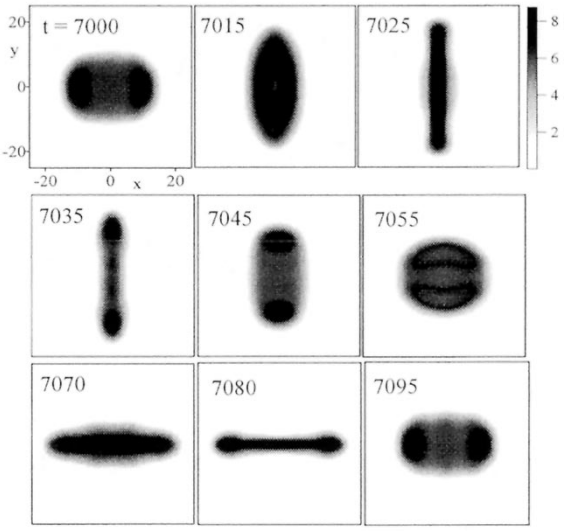

Fig. 9. Dynamics of transverse intensity distribution during one oscillation cycle of the transient regime. The initial field is the fundamental laser soliton formed at $g_0 = 2.1140$, then gain is increased slowly up to $g_0 = 2.1145$ and, finally, the initial gain value is restored ($g_0 = 2.1140$).

velocity. The latter soliton is axially asymmetric and has two intensity maxima (a two-humped structure, Fig. 8, $t = 800$). More precisely, a stationary rotating soliton can be formed if gain first increases above the stability threshold and then decreases to a value corresponding to the range of this soliton stability (see Fig. 10). The rotation is connected with the asymmetry of the transverse distribution of the complex electric-field envelope and is not related to the structure topological charge. The localized structures shown in Fig. 8 have no vortices. Such rotating laser solitons were first found in [25]. Below, we will give new examples of rotating solitons and study their bifurcations. Note that Fig. 8 corresponds to the fast gain increase. If it is slow, then a metastable nonrotating localized structure arises that oscillates quasi-periodically. One of the oscillation cycles of the almost periodic antiphase pulsation of x and y sizes of the structure is shown in Fig. 9. There are two symmetry axes, x and y, for the field distributions. More than 100 oscillation cycles occur during the metastable state lifetime. Then the structure loses its symmetry and transforms into a stable rotating soliton.

For the parameters of Fig. 3, there is a hysteresis between stationary fundamental solitons and asymmetric rotating solitons. Coexistence of the two branches of stable solitons is shown in Fig. 10 where widths [Fig. 10(a)] and intensities [Fig. 10(b)] of solitons are given as functions of small-signal gain. The two widths of the rotating soliton are determined as the temporal maximum and minimum over the rotation period at the level of the intensity of the transversely homogeneous lasing. This level is indicated in Fig. 10(b) by the dashed line.

The rotating soliton arising after the Andronov–Hopf bifurcation bifurcates again with a further gain increase. At $g_0 = 2.117$, it transforms into a new structure — a pulsating rotating asymmetric laser soliton. Then the curves representing the maximum and minimum widths [Fig. 10(a)] and maximum intensity [Fig. 10(b)] split due to time-periodic oscillations that are slow compared with the rotation period. With the gain decrease, the rotating soliton persists over a narrower range as compared with

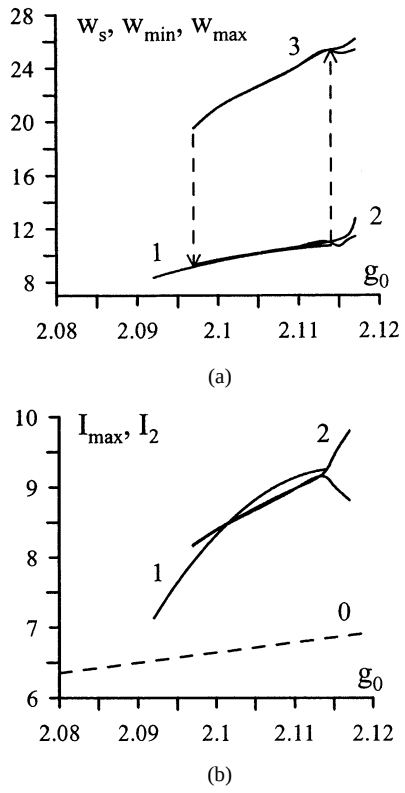

Fig. 10. Dependencies of (a) soliton widths w and (b) intensities I on the small-signal gain g_0. The 1 (a) and 2 (b) curves correspond to a stable axially symmetric soliton with width w_s and maximum intensity I_2. Curves 2 and 3 in both (a) and (b) indicate the maximum and minimum values of w and I for an asymmetric rotating soliton. Curve 0 (b) shows the intensity of the transversely homogeneous lasing. The splitting of the curves corresponds to temporal pulsations of the width and the maximum intensity of the asymmetric rotating and pulsating soliton that appears after the Andronov–Hopf bifurcation; $d = 0$.

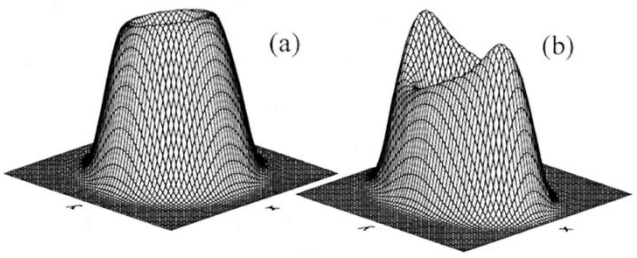

Fig. 11. Transverse intensity distributions for rotating one- and two-humped localized laser vortices. $m = 1$, $d = 0.06$, (a) $g_0 = 2.13$, (b) $g_0 = 2.09$.

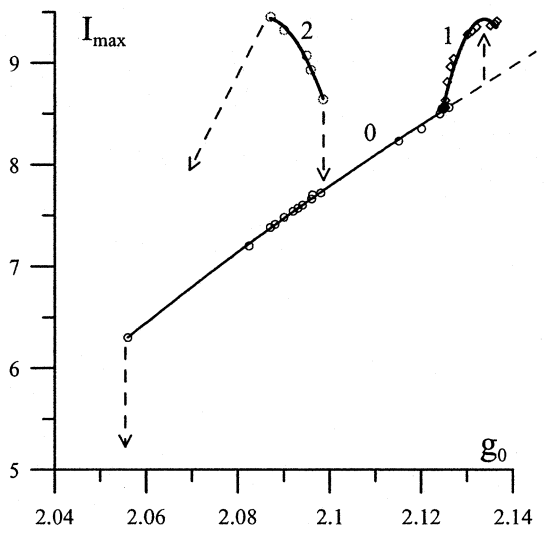

Fig. 12. Maximum intensity of stable symmetric and asymmetric laser localized vortices versus the small-signal gain. Curves 0, 1, and 2 correspond to symmetric, $m = 1$, asymmetric one-humped and asymmetric two-humped vortices, respectively. Vertical dashed lines with arrows represent hysteresis jumps that take place with gain variation. The oblique dashed line indicates a jump to a regime with the soliton splitting into two decaying localized fragments; $d = 0.06$.

the fundamental soliton characterized by axially symmetric intensity distribution. With the decrease of gain, a rotating soliton becomes unstable, and the transition to the fundamental soliton occurs. In Fig. (10a), this transition is shown by the downward arrow.

For laser vortices $(m \neq 0)$, both high- and low-gain boundaries of the stability range correspond to the Andronov–Hopf bifurcations (see Figs. 5–7). Numerical simulations of the laser vortex destabilization give a wide spectrum of stable localized structures. It would appear reasonable that the Andronov–Hopf bifurcation results in the formation of a rotating soliton with the number of maxima equal to the value δm of the perturbation responsible for the instability. However, this conclusion is not universally valid, because the linear stability analysis does not describe the nonlinear stage of perturbation growth.

The symmetric vortex of the first order, $m = 1$, is associated with two types of stable rotating asymmetric solitons: two-humped solitons existing in the low-gain region and one-humped solitons in the high-gain region (Fig. 11). Note that the formation of the one-humped soliton cannot be explained by the results of the linear stability analysis (see Fig. 5). The coexistence of different solitons and hysteresis jumps between them with gain variations are shown in Fig. 12. With the increase of gain, the initially symmetric localized vortex loses its symmetry and transforms into a rotating one-humped soliton. With a further increase in the gain, this soliton also loses its stability. Then, after an intermediate metastable regime of oscillations, the lasing zone progressively widens in the form of a cylindrical switching wave [20].

With the decrease of gain, the one-humped rotating soliton transforms into a vortex soliton with the axially symmetric intensity distribution. There exists an extremely narrow hysteresis range where both types of solitons coexist. The hysteresis range is fairly wide in the low-gain region where symmetric vortices coexist with two-humped solitons (Fig. 12). Note that, in this case, two-humped solitons cannot be formed from symmetric vortices by a slow gain variation, but they can be excited by a sufficiently strong asymmetric perturbation.

Further decrease of gain results in splitting of both symmetric and asymmetric (rotating) vortex solitons into two fragments without dislocations. Then these fragments disappear. This process is illustrated in Fig. 13, where the transverse distributions of intensity and phase are given for different time moments. The sharp change of the phase corresponds to its 2π jump at the line starting from the dislocation center where the radiation intensity is zero.

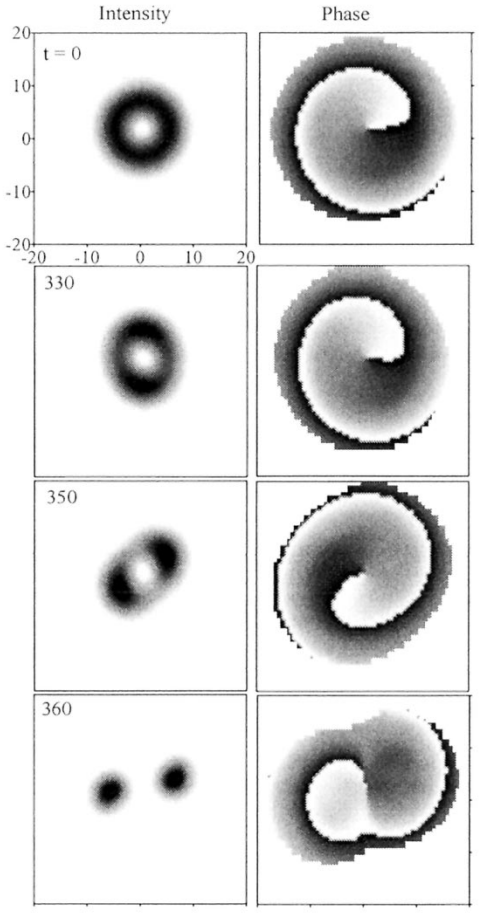

Fig. 13. Breakdown of the symmetric laser vortex soliton with $m = 1$ occurring at an abrupt decrease of the small-signal gain from 2.054 to 2.05; $d = 0.06$.

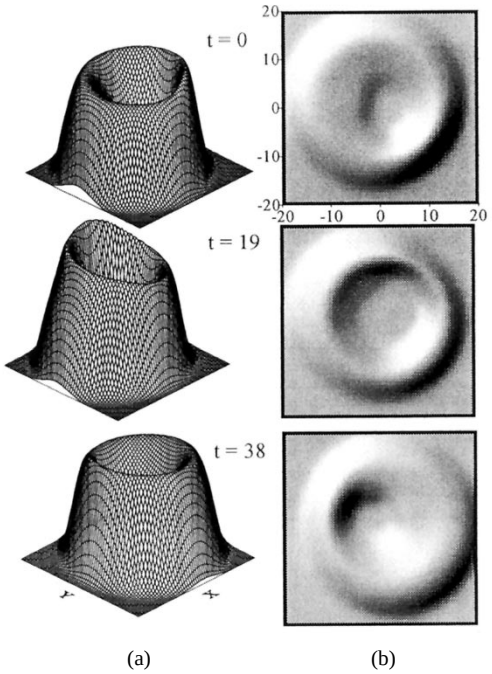

(a) (b)

Fig. 14. (a) Wired surfaces and (b) surface reliefs illustrating the transverse distribution of intensity of a rotating and simultaneously oscillating laser vortex; $m = 2, g_0 = 2.115, d = 0.06$; distribution is approximately periodic with the period $T \approx 38$.

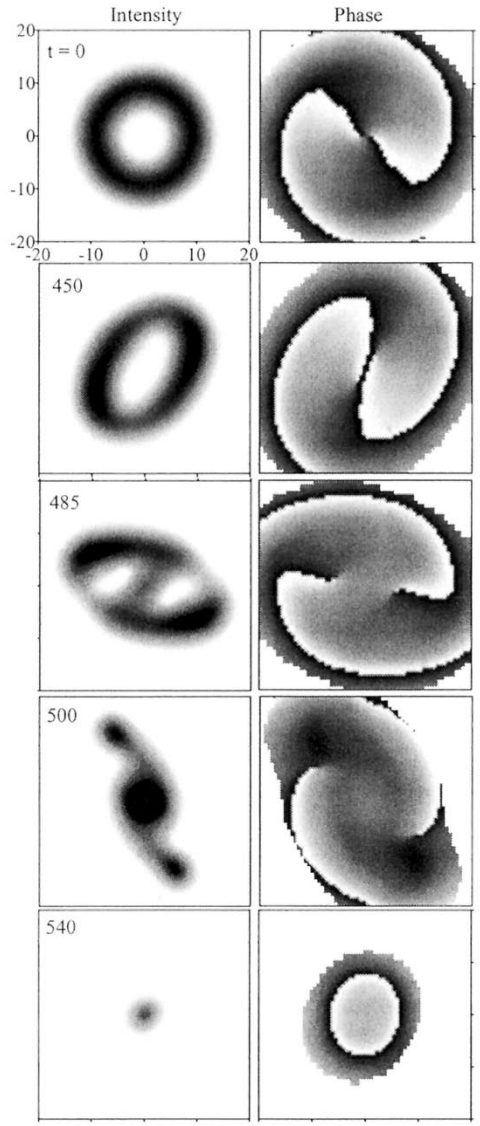

Fig. 15. Breakdown of the symmetric laser vortex soliton with $m = 2$ occurring at an abrupt decrease of the small-signal gain from 2.057 to 2.056; $d = 0.06$.

Similar or even more complex are bifurcations of higher order localized vortices. In this case, stable rotating and simultaneously oscillating solitons (Fig. 14, $m = 2$) exist within a fairly wide range of gain. In Fig. 15, we demonstrate the breakdown of the symmetric second-order laser vortex with $m = 2$ into two vortices of the first order $(t = 485)$ and their further splitting and decay. In the case of breakdown of the rotating asymmetric soliton (Fig. 16), the fragments arising from the vortex splitting have a rather large relative velocity. It can be attributed to the initial angular momentum, which is absent in the case of the symmetric vortex shown in Fig. 13.

Bifurcations of the third-order vortices, $m = 3$, are even more varied. Without going into detail, we simply present in Fig. 17 the stable state of a rotating asymmetric vortex with three intensity maxima. The number of the maxima corresponds to the value $\delta m = 3$ of the perturbation associated with the bifurcation of the symmetric laser vortex that takes place with the decrease of gain (see Fig. 7).

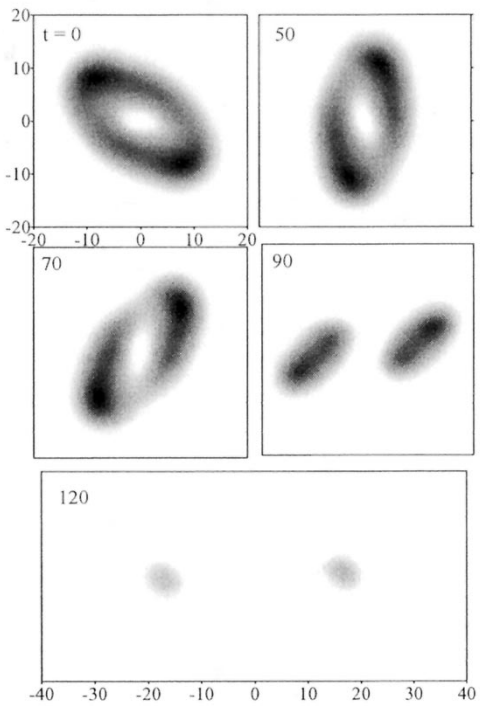

Fig. 16. Transverse intensity distributions illustrating the breakdown of the asymmetric rotating laser localized vortex ($m = 2$). The breakdown occurs at an abrupt decrease of the small-signal gain from 2.083 to 2.082, $d = 0.06$.

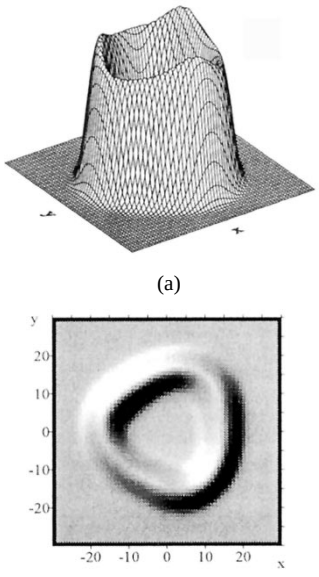

(a)

(b)

Fig. 17. (a) Wired surface and (b) surface relief illustrating the transverse intensity distribution of a rotating triple-humped laser vortex; $m = 3$, $g_0 = 2.0869$, $d = 0.1$.

V. Conclusion

The results presented demonstrate a great variety of dissipative solitons in wide-aperture lasers with a saturable absorber. Even more diverse are the forms of solitons in bistable class-B lasers where finite relaxation rates of gain and absorption should be taken into consideration. It would appear reasonable that this rich variety can be used in designs of such devices as a shift register and optical adder [20], as well as other devices for optical information processing.

Let us take a brief look at the experimental realization of the solitons considered in this paper. Until recently, experiments with laser solitons were made with extremely slow absorbers. To get fast systems that can be integrated with other information processing devices, it is natural to use the semiconductor vertical cavity surface-emitting lasers (VCSELs) with a saturable absorber integrated in the same semiconductor device of a micron in size. The saturable absorber could consist of passive layers with multiple quantum wells or dots. The electrodes necessary for laser pumping by the electric current should be placed between the active and passive layers. They should be transparent to light. Such laser devices could be complementary to the semiconductor passive driven interferometers of the type reviewed in [15] and [19].

Acknowledgment

The second author would like to thank V. B. Taranenko and C. O. Weiss for the acquaintance with [19] prior to its publication.

References

[1] V. E. Zakharov, S. V. Manakov, S. P. Novikov, and L. P. Pitaevskii, *Theory of Solitons: The Inverse Scattering Method*. New York: Plenum, 1984.

[2] A. C. Newell, *Solitons in Mathematics and Physics*. Philadelphia, PA: SIAM, 1987.

[3] N. N. Akhmediev and A. Ankiewicz, *Solitons*. London, U.K.: Chapman and Hall, 1997.

[4] N. N. Rosanov and G. V. Khodova, "Autosolitons in bistable interferometers," *Opt. Spectrosc.*, vol. 65, no. 6, pp. 449–450, 1988.

[5] N. N. Rosanov, A. V. Fedorov, and G. V. Khodova, "Effects of spatial distributivity in semiconductor optical bistable systems," *Phys. Stat. Sol. B*, vol. 150, no. 2, pp. 545–555, 1988.

[6] A. N. Rakhmanov, "Transverse diffraction structures in optical feedback systems," *Opt. Spectrosc.*, vol. 74, no. 6, pp. 701–702, 1993.

[7] A. N. Rakhmanov and V. I. Shmalhausen, "Optical memory device based on the phenomenon of optical transversal autosolitons," *Proc. SPIE*, vol. 2108, pp. 428–434, 1993.

[8] B. Schapers, M. Feldmann, T. Ackemann, and W. Lange, "Interaction of localized structures in an optical pattern-forming system," *Phys. Rev. Lett.*, vol. 85, no. 4, pp. 748–751, 2000.

[9] N. N. Rosanov and S. V. Fedorov, "Diffractive switching waves and autosolitons in laser with saturable absorber," *Opt. Spectrosc.*, vol. 72, no. 6, pp. 1394–1399, 1992.

[10] S. V. Fedorov, G. V. Khodova, and N. N. Rosanov, "Soliton-like field transverse structures in passive and active optical bistable systems," *Proc. SPIE*, vol. 1840, pp. 208–215, 1992.

[11] V. Y.V. Yu. Bazhenov, V. B. Taranenko, and M. V. Vasnetsov, "Transverse optical effects in bistable active cavity with nonlinear absorber on bacteriophodopsin," *Proc. SPIE*, vol. 1840, pp. 183–193, 1992.

[12] F. T. Arecchi, S. Bocaletti, and P. Ramazza, "Pattern formation and competition in nonlinear optics," *Phys. Rep.*, vol. 318, no. 2, pp. 1–83, 1999.

[13] L. A. Lugiato, M. Brambilla, and A. Gatti, "Optical pattern formation," in *Advances in Atomic, Molecular, and Optical Physics*, B. Bederson and H. Walther, Eds. Boston, MA: Academic, 1999, vol. 40, pp. 229–306.

[14] C. O. Weiss, M. Vaupel, K. Staliunas, G. Slekys, and V. B. Taranenko, "Vortices and solitons in lasers," *Appl. Phys. B: Laser Opt.*, vol. 68, no. 2, pp. 151–168, 1999.

[15] C. O. Weiss, G. Slekys, V. B. Taranenko, K. Staliunas, and R. Kuszelewicz, "Spatial solitons in resonators," in *Spatial Solitons*, S. Trillo and W. E. Torruellas, Eds. Berlin, Germany: Springer-Verlag, 2001, pp. 393–414.

[16] W. J. Firth, "Theory of cavity solitons," in *Soliton-Driven Photonics*, A. D. Boardman and A. P. Suchorukov, Eds. Dordrecht, The Netherlands: Kluwer, 2001, pp. 459–485.

[17] W. J. Firth and G. K. Harkness, "Existence, stability and properties of cavity solitons," in *Spatial Solitons*, S. Trillo and W. E. Torruellas, Eds. Berlin, Germany: Springer, 2001, pp. 343–358.
[18] W. J. Firth and C. O. Weiss, "Cavity and feedback solitons," *Opt. Photon. News*, vol. 26, no. 2, pp. 54–58, 2002.
[19] V. B. Taranenko and C. O. Weiss, "Spatial solitons in semiconductor microresonators," *J. Select. Topics Quantum Electron.*, vol. 8, pp. 488–496, May/June 2002.
[20] N. N. Rosanov, *Spatial Hysteresis and Optical Patterns*. Berlin, Germany: Springer-Verlag, 2002.
[21] D. Michaelis, V. Peschel, and F. Lederer, "Multistable localized structures and superlattices in semiconductor optical resonators," *Phys. Rev. A*, vol. 56, no. 5, pp. R3366–R3369, 1997.
[22] L. Spinelli, G. Tissoni, M. Brambilla, F. Prati, and L. A. Lugiato, "Spatial solitons in semiconductor microcavities," *Phys. Rev. A*, vol. 58, no. 3, pp. 2542–2559, 1998.
[23] A. F. Suchkov, "Effect of inhomogeneities on the operation regime of solid-state lasers," *Sov. Phys. JETP*, vol. 22, no. 5, pp. 1026–1031, 1966.
[24] S. V. Fedorov, A. G. Vladimirov, G. V. Khodova, and N. N. Rosanov, "Effect of frequency detunings and finite relaxation rates on laser localized structures," *Phys. Rev. E*, vol. 61, no. 5, pp. 5814–5824, 2000.
[25] N. N. Rosanov, A. V. Fedorov, S. V. Fedorov, and G. V. Khodova, "New types of localized structures of laser radiation," *Opt. Spectrosc.*, vol. 79, no. 5, pp. 795–797, 1995.
[26] L.-C. Crasovan, B. A. Malomed, and D. Michalache, "Stable vortex solitons in the two-dimensional Ginzburg-Landau equation," *Phys. Rev. E*, vol. 63, p. 016 605, 2001.
[27] A. G. Vladimirov, N. N. Rosanov, S. V. Fedorov, and G. V. Khodova, "Bifurcation analysis of laser autosolitons," *Quantum Electron.*, vol. 27, no. 11, pp. 949–952, 1997.
[28] ——, "Analysis of the stability of laser solitons," *Quantum Electron.*, vol. 28, no. 1, pp. 55–57, 1998.
[29] S. V. Fedorov, N. N. Rosanov, A. N. Shatsev, N. A. Veretenov, and A. G. Vladimirov, "Oscillating and rotating states for laser solitons," *Proc. SPIE*, vol. 4751, pp. 471–477, 2002.

Sergey V. Fedorov was born in St. Petersburg, Russia, in 1956. He received the degree in physics from St. Petersburg State University in 1979.

He joined the Theoretical Department of the Vavilov State Optical Institute in 1979, where he has been engaged in the research of laser systems. He is currently a Senior Research Scientist with the Theoretical Department of the Research Institute for Laser Physics, St. Petersburg, Russia. He is the author or coauthor of over 50 papers in the field of laser physics.

Nikolay N. Rosanov was born in St. Petersburg, Russia, in 1940. He received the degree in physics from St. Petersburg State University in 1963, and the Cand.Phys. and Doct.Phys. degrees from the Vavilov State Optical Institute, St. Petersburg, in 1970 and 1983, respectively.

He joined the Vavilov State Optical Institute in 1963, where he was engaged in research in laser physics and nonlinear optics. He is currently Head of the Theoretical Department of the Research Institute for Laser Physics, St. Petersburg, and also a Professor at the St. Petersburg State Institute of Fine Mechanics and Optics (Technical University). He is the author or coauthor of over 200 papers and several books published in Russian and in English.

Dr. Rosanov is a member of the Russian and American Optical Societies, the SPIE, and the Board of National Experts of the Union of Independent States (former USSR) in lasers and laser technology.

Anatoly N. Shatsev was born in St. Petersburg, Russia, in 1947. He received the degree in physics from St. Petersburg State University in 1971, and the Cand. Phys. degree from the Vavilov State Optical Institute, St. Petersburg, in 1989.

He joined the Theoretical Department of the Vavilov State Optical Institute in 1971, where he was engaged in research on laser systems. He is currently a Senior Research Scientist with the Theoretical Department of the Research Institute for Laser Physics, St. Petersburg.

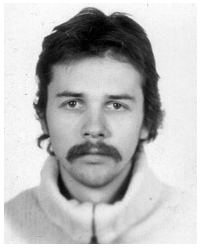

Nikolay A. Veretenov was born in St. Petersburg, Russia, in 1977. He received the B.S. degree in physics in 2000 from St. Petersburg State University, where he is currently working toward the M.S. degree.

His research focuses on laser solitons.

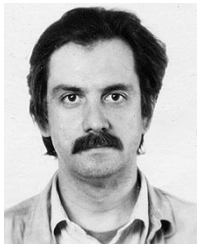

Andrei G. Vladimirov was born in St. Petersburg, Russia, in 1958. He received the Ph.D. degree from St. Petersburg State University, St. Petersburg, Russia, in 1984.

He is currently an Associate Professor in the Department of General Physics, St. Petersburg State University. His research interests include nonlinear dynamics in lasers and laser systems, localized structures of light, optical solitons.

Dr. Vladimirov is a member of the Russian Optical Society.